IEEE Access
Multidisciplinary | Rapid Review | Open Access Journal

Received January 28, 2021, accepted February 4, 2021, date of publication February 10, 2021, date of current version February 25, 2021.

*Digital Object Identifier 10.1109/ACCESS.2021.3058619*

# Evolutionary Algorithms for 5G Multi-Tier Radio Access Network Planning

**HASSANA GANAME[1], LIU YINGZHUANG[1], AYMEN HAMROUNI[2], (Student Member, IEEE), HAKIM GHAZZAI[2], (Senior Member, IEEE), AND HUA CHEN[3]**

[1]School of Electronics and Information Engineering, Huazhong University of Science and Technology, Wuhan 430074, China
[2]School of Systems and Enterprises, Stevens Institute of Technology, Hoboken, NJ 07030, USA
[3]College of Mathematics and Computer Science, Wuhan Textile University, Wuhan 430073, China

Corresponding author: Hua Chen (chenhua@wtu.edu.cn)

**ABSTRACT** With the ever-increasing traffic demand of wireless users, resulting from the huge deployment of Internet-of-Things (IoT) devices and the emergence of smart city applications requiring ultra-low latency networks, the Fifth Generation (5G) of cellular networks have been introduced as a revolutionary broadband technology to boost the quality of service of mobile users. In this paper, we investigate the planning process for a 5G radio access network having mmWave Micro Remote Radio Units (mRRUs) on top of sub-6 GHz Macro Remote Radio Units (MRRUs). We rely on proper channel models and link budgets as well as Urban Macro-cells (UMa) and Urban Micro-cells (UMi) characteristics to carefully formulate a 5G network planning optimization problem. We aim to jointly determine the minimum number of MRRUs and mRRUs to install and find their locations in a given geographical area while fulfilling coverage and user traffic demand constraints. In order to solve this planning process, we propose a two-step process where we first employ a low complexity meta-heuristic algorithm to optimize the locations of RRUs followed by an iterative elimination method to remove redundant cells. To evaluate the performances of this proposed approach, we conduct a comparative study using Accelerated Particle Swarm Optimization and Simulated Annealing. Simulations results using sub-6 GHz UMa and 28 GHz UMi demonstrate the ability of the proposed planning approach to achieve more than 98% coverage with minimum cell capacity outage rate, not exceeding the 2%, for different scenarios and illustrate the efficiency of the evolutionary algorithms in solving this NP-hard problem in reasonable running time.

**INDEX TERMS** 5G networks, radio heterogeneous network planning, network dimensioning, swarm intelligence, evolutionary algorithm.

## I. INTRODUCTION

The demand for mobile data traffic and higher access rate in last decade have been significantly increasing due to the increase of number of Internet-of-Things (IoT) devices and the emergence of several applications requiring low-latency and real-time access (e.g., autonomous vehicles systems [1], financial trading [2], mobile crowdsourcing [3], playback streaming [4], etc). The previous broadband cellular network generation, the Fourth Generation (4G), specifically Long-Term Evolution Advanced (LTE-A) [5], [6], is no more providing sufficient capacities to meet our nowadays bandwidth and latency demands. In the IoT [7] context, 4G technology has not been successful in enabling IoT real-time transmission (i.e., below 5ms latency). The technology behind it was designed to only allow packet switching IP-based connectivity which has high processing, queuing, transmission, and propagation delays. Furthermore, the battery support for the devices has not been fully met as energy consumption [8] in the 4G architecture remains very high.

The Fifth Generation (5G) of wireless networks was proposed as a solution to surpass these limitations and cover these requirements through different scenarios such as ultra-high traffic, ultra-high connection, and ultra-high mobility [9]. Unlike previous generation, 5G architecture is designed in such a way that it can take advantage of cloud-based or virtual Radio Access Networks (RANs) cellular systems [10]. It supports ultra-low power, long-life battery, and always connected IoT devices. The 5G encompasses frequencies from around 500 MHz up to 100 GHz which can

The associate editor coordinating the review of this manuscript and approving it for publication was Ding Xu.

meet the traffic demand and provide fast access by delivering high data rate, expanding coverage, and introducing network facility in all equipment of mobile communication systems [11]–[14]. 5G radio frequency bands are wider than those of previous generations of cellular networks. The 5G uses cognitive radio techniques to differentiate each device and offer appropriate delivery channel. Its network introduces different components from the previous generations, mainly due to virtualization and service-based architectures. Massive Multiple Input Multiple Output (MIMO) and hybrid beamforming are core techniques to achieve the targeted high data rates and the large number of devices. Also, they are designed to support considerably higher data rates, very large numbers of connected IoT devices, and enable low latency while providing adaptive means for network scalability and flexibility.

The transition to 5G communication standards is not an instantaneous process. It requires careful preparation and preliminary planning. It is necessary to update both the data transmission network and the subscriber radio access network. Since the transition process will be carried out within the network serving subscribers, it is necessary to develop approaches that make the network resource updates transparent for customers and with minimal costs for mobile operators. Because the 5G comes with a high installation budget and an exponential growth of mobile data services usage, rethinking the network planning strategies, which was proven to be an NP-hard problem, becomes essential for optimized placement of the radio access networks. The 5G New Radio (NR), which describes the interface and radio access technology for cellular networks, proposes new spectrum bands ranging from Frequency Range 1 (FR1), including sub-6 GHz frequency mid bands, to Frequency Range 2 (FR2), including frequency high bands in the mmWave range (24–100GHz). The advanced antenna techniques that are being introduced with 5G NR has motivated the usage of mmWave carrier frequencies. mmWave offers a large amount of available unlicensed spectrum that allows better cell-edge coverage, large bandwidth (BW), less interference caused by the neighboring cells transmission as compared to microwave, and more importantly frequency reuse within a short distance. This being said, using the mmWave bands in 5G results in higher bandwidth but also a limited coverage that can only be surpassed by a huge network densification involving massive distributions of Remote Radio Units (RRUs) across the region of interest. This certainly leads to higher installation cost and maintenance. On the other hand, relying on sub-6 GHz RRUs results in wider network coverage, consequently lower cost, but this comes with a limitation in the network bandwidth since sub-6 GHz bands operates with limited bandwidth.

Typically, the cell deployment architectures can be classified into standalone and heterogeneous architectures. In the context of 5G, the former refers to a network deployment that consists of mere mmWave small cells, while the latter refers to the deployment of mmWave small cells on top of the existing macro-relay networks in the form of hierarchical

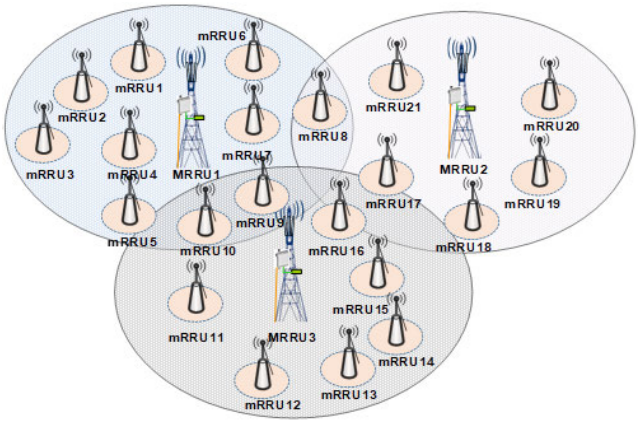


**FIGURE 1.** Explanatory figure illustrating an example of a two-tier heterogeneous architecture with macro- and micro- cells.

or mixed cell structures. In the heterogeneous architecture, the macrocell layer is mainly for coverage as well as mobility and signaling problems originating from the mmWave small-cell layer, which exists for capacity boosts. The much wider bandwidth as well as the beamforming/MIMO capabilities, together with the reduced access-link distances, enable the mmWave small cells with the capability to substantially increase the system capacity.

In this paper, we study the planification of a heterogeneous network architecture, which consists in the deployments of sub-6 GHz spectrum Urban Macro-cells (UMa) RRUs, referred to as MRRUs, under the coverage of a mmWave Urban Micro-cells (UMi) RRUs, referred to as mRRUs. The UMi antennas provide high data rate with a limited short range coverage while the UMa antennas allow a long range coverage. An explanatory example of a possible macro-micro architecture is included in Fig. 1 where MRRUs and mRRUs must be placed carefully to satisfy the coverage and bandwidth constraints. The proposed architecture studies the trade-off between: 1) massive mRRUs implementation leading to better Quality of Service (QoS) and installation cost and 2) low MRRUs implementation leading to poor QoS and low implementation cost. Our study aims to define a hybrid approach where we find the minimum number as well as the locations of required MRRUs and mRRUs to be installed in a region of interest while satisfying the user traffic demand requirement and coverage constraints in the planning process. In order to achieve this, we proceed with the following steps:

1) At first, we define appropriate system parameters and users' requirements for a given geographical area. The latter can be decomposed into multiple subareas characterized by different density and distribution of users. We rely on 3GPP standard and exploit the Frequency Range 1 (FR1), specifically 6 GHz, in the planning process for the MRRUs and Frequency Range 2, with carrier frequency 28 GHz, in the planning process for the mRRUs.
2) After defining the appropriate system parameters, we perform preliminary coverage and cell capacity

dimensioning phases to determine an initial number of MRRUs and mRRUs that, separately, can satisfy the targeted QoS.

3) Then, we proceed with a joint placement phase of the MRRUs and mRRUs to determine their optimized locations such as coverage and targeted DownLink (DL) and UpLink (UL) data rates are satisfied. To this end, and after formulating a suitable optimization problem, we design a two-stage meta-heuristic approach to deal with the NP-hard network planning problem. Two modified evolutionary algorithms, namely the Simulated Annealing (SA) and the Accelerated Particle Swarm Optimization (A-PSO) algorithms, are developed to separately determine the optimized locations of MRRUs and mRRUs.
4) Finally, an iterative approach is designed to eliminate redundant MRRUs and mRRUs while maintaining the required coverage level and provided data rate per each subarea.

To evaluate the performances of the proposed architecture, a comparative study between A-PSO and SA is conducted for different planning scenarios. A Monte Carlo simulation is also executed to asses the performance of the developed model. The simulations results demonstrate that essential gains could be achieved using the proposed planning approach, which allows satisfaction of the targeted coverage and QoS with rapid convergence. It is shown that the cell capacity outage rate did not exceed the 2% level for the investigated with almost 100% coverage. The proposed approach is generic and scalable and takes into account most of the aspects related to network planning including 5G link budgets, channel propagation and atmospheric attenuation models, sectorisation, duplex mode, as well as various user densities and distributions and QoS requirements. It can be applied to any scenario and can be easily extended to multi-tier heterogeneous networks.

The remainder of this paper is organized as follows. Related work is reviewed in Section II. An explanatory description of the multi-tier heterogeneous architecture is discussed in Section I. The system model and dimensioning phases are presented in Section IV. Problem formulation for solving the mRRUs and MRRUs placement is introduced in Section V. Section VI presents the proposed low complexity approach for placing the minimum number of MRRUs/mRRUs and determining their optimized locations. Experiments and evaluations are discussed in Section VII and finally, in Section VIII, we conclude this paper and shed the light on future research directions.

## II. RELATED WORK

The network planning problem has been widely investigated in the previous generations scenarios [5], [15]–[19]. For example, LTE cell planning was investigated in [20] where the authors proposed to adjust eNodeB locations based on a stochastic approach. greedy Base Stations (BSs) deployment algorithm was proposed by the authors in [21] to find the optimized location of BSs to be deployed. The deployment is based on the center of the region to avoid the influence of the cell edge effect. SA is proposed in [18] to explore the placement of BSs. After finding the input parameters and the number of BSs in LTE networks, the authors investigated the placement for different user distribution in the area of interest.

Because of the 5G standard limited range resulting from its short wavelength, the theoretical expected amount of mRRUs that needs to be deployed in the cellular network is massive. Therefore, the planning process is critical and needs to be deeply rethought. Most of the existing studies [22]–[25] discussed standalone planning for mRRUs. For instance, in [26], the energy efficiency prospects of 5G wireless networks are analyzed for reducing energy consumption in different parts of the networks. The work in [27] introduced an analytical model for planning and dimensioning of 5G cloud RAN in the context of energy efficiency. Other studies investigated 5G network planning and deployments from different perspectives. For instance, in [28], a model for choosing an optimal place of the base station to maximize the coverage area for different 5G frequencies in an urban scenario was presented. On the other hand, [29] introduced an in-house open-source techno-economic assessment tool for 5G deployments [30] in macro-cell scenarios to minimize the cost through infrastructure sharing strategies. In [17], the authors studied the coverage and capacity dimensioning procedures to optimize the 4G LTE networks for the upcoming 5G deployments in the non-standalone scenario, while considering capacity and coverage planning. The authors in [31] proposed to optimize the deployment of edge devices in 5G networks while maximizing service quality, reliability, and minimizing cost and energy consumption. In [32], a detailed technical and economic analysis to minimize the 5G deployment cost in the context of different architectural scenarios was presented. However, the study lacks the discussion on coverage, capacity, and quality of service. The authors of [33] proposed a standalone 5G architecture exclusively employing mmWave signals. A recent work [34] studied the 5G network planning as a profit maximization model for the mobile network operator with minimal deployment cost. Ultra-dense 5G deployment was investigated in [35] where the authors proposed a non-dominated sorting genetic algorithm to solve the cell planning problem. Similarly, the authors of [36] proposed to increase the number of antennas and to use higher sectorisation in order to satisfy user traffic demand in the ultra-dense deployment process in mmWave band. The authors of [37] evaluated the deployment of ultra-dense network with different BSs at different frequencies ranging from 2 GHz to 60 GHz. The location of BSs in the cell planning process in a real scenario with respect to user data rates requirements and cell coverage constraints was not discussed.

The above revision of the existing literature suggests that, to the best of our knowledge, our work is the first that developed a micro-macro cells 5G heterogeneous network planning that incorporates NR numerology and bandwidth

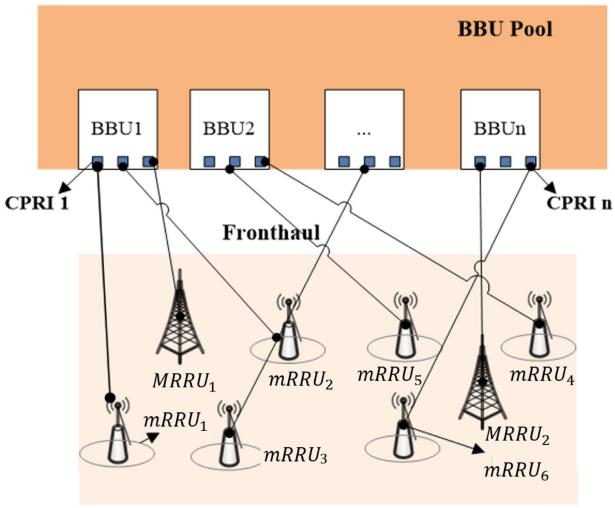


**FIGURE 2.** High-level illustration showing the front-haul of a 5G network.

parts with cross-tier interference between sub-6 GHz and mmWave frequencies where we jointly determine the number and locations of MRRUs and mRRUs and afterwards, eliminate redundant MRRU/mRRUs.

## III. 5G FRONTHAUL ARCHITECTURE

The 5G networks are in the process of revolutionizing the telecommunication industry by providing the newest technologies and architectures such as mmWave, massive-MIMO, HetNet, full-duplex systems, Cloud RAN (C-RAN), etc. A multi-tier architecture authorizes subscribers in various tier to have various precedencies for channel access and various types of connections, small cells connections, and macrocells connections, thus supporting low latency and high data rates. Fig. 2 shows the fronthaul of the 5G network architecture including macro-cells, small cells, RRUs, Base Band Unit (BBU). As illustrated in the figure, the fronthaul corresponds to the connection between the RRUs and BBUs in both directions. The backhaul, which is not illustrated in the figure, essentially consists in the connection between the BBU and the core network in both directions. The digital baseband signal travels from the BBU to a RRU through a Digital Radio-over-Fiber (DRoF) connection. The RRU converts the received radio frequency (RF) of the uplink signal from the User Equipment (UE) into a digital baseband signal. The whole area network is divided into the microcells and macrocells leading to a multi-tiered network architecture. mRRU Densification reduces the load on MRRUs while providing better end-to-end latency in communication. They also increase energy efficiency since the mRRUs consume lower power than those of MRRUs. All the RRUs are connected to the BBU pool via Common Public Radio Interface (CPRI) ports. MRRUs are represented by sub-6 GHz radio units while mRRUs are represented by mmWave radio units. RRUs are used in this model instead of the Radio Frequency Unit (RFU) to reduce the cable loss (i.e., the feeders are replaced by fibers). In this model, MRRUs are deployed to provide coverage for the area and to support low-level traffic demand, whereas, mRRUs manage low-coverage and high-level data rate demand. In this paper, our aim is to perform the planning process in such a multi-tier heterogeneous architecture where we focus on simultaneously optimizing the number and locations of MRRUs and mRRUs.

**TABLE 1.** List of notations.

| Notations | Descriptions |
|---|---|
| UMa | Urban macro cells |
| UMi | Urban micro cells |
| MRRUs, mRRUs | Macro, micro remote radio units |
| $S^i_{\text{RRU}}$ | The set of RRUs with type $i$ |
| $R^i_{\text{RRU}}$ | The radius of cell with type $i$ |
| $S$ | The total surface of served area |
| $S_p$ | The total surface of subarea $p$ |
| $D_p(x, y)$ | Probability density of subarea $p$ |
| $N^i_{\text{Cov}}$ | The number of RRUs, having type $i$, needed to satisfy the coverage constaints |
| $N^i_{\text{Cap}}$ | The number of RRUs, having type $i$, needed to satisfy the capacity constaints |
| $N^i_U$ | Maximum number of users that can be served by one MMRU or mRRU |
| $N^i_{\text{Dim}}$ | Initial number of RRUs that satisfies the QoS |
| $\text{MAPL}^i_x$ | Maximum allowed path loss for cell type $i$ in propagation direction $x$ |
| $PL^{\text{UMa}}$ | Path loss model in NLOS for UMa cells |
| $PL^{\text{UMi}}$ | Path loss model in LOS for UMi cells |
| $S^i_{\text{Cell}}$ | Surface of cells with type $i$ |

**TABLE 2.** MRRU and mRRU specifications [38].

| Specifications | MRRU | mRRU |
|---|---|---|
| Frequency Range | FR1-sub-6 GHz | FR2- mmWave |
| Band | n96 | n257 |
| Frequency | 6 GHz | 28 GHz |
| Sub-carrier Bandwidth | 60 kHz | 240 kHz |
| Duplex Mode | TDD | TDD |
| UL-DL Range | 5925 – 7125 MHz | 26.50 – 29.50 MHz |
| Channel Bandwidths | 20, 40, 60, 80 | 50, 100, 200, 400 |
| Selected Bandwidth | 20 MHz | 100 MHz |

## IV. SYSTEM PARAMETERS AND DIMENSIONING

In this section, we define the system model and parameters needed for the 5G RRU planning optimization problem. This study aims to define a hybrid approach where we jointly find the minimum number as well as the locations of MRRUs and mRRUs to be installed in a region of interest while satisfying the user traffic demand requirement and coverage constraints. At first, we start by introducing suitable

**TABLE 3.** MRRUs and mRRUs parameters.

| | MRRU | mRRU |
|---|---|---|
| **Transmit Power ($A$):** | 49 dBm | 35 dBm |
| **Cable and connector loss ($B$):** | 2 dB | 2 dB |
| **Send Antenna gain ($C_1$)** | 11 dBi | 7 dBi |
| **Receive Antenna gain ($C_2$)** | 4 dBi | 18 dBi |
| **Temperature ($E$)** | 290.0 $K$ | 290.0 $K$ |
| **Bandwidth ($F$)** | 20 MHz | 100 MHz |
| **Interference margin ($M$)** | 2 dB | 2 dB |
| **Mast head amplifier ($N$)** | 2 dB | 2 dB |
| **Cable loss ($O$)** | 3 dB | 3 dB |
| **Height** | 20 m | 7 m |

**TABLE 4.** UE parameters.

| | UE |
|---|---|
| **Transmit power ($A'$)** | 24 dBm |
| **Cable and connector loss ($B'$)** | 0 dBm |
| **Send antenna gain ($C'_1$)** | 0 dBi |
| **Recieve antenna gain ($C'_2$)** | 0 dBi |
| **Temperature ($E'$)** | 290.0 K |
| **Bandwidth ($F'$)** | 10 MHz |
| **Interference margin ($M'$)** | 3 dB |
| **Control channel share ($N'$)** | 1 dB |
| **Body loss ($O'$)** | 0 dB |
| **Heights** | 1.6m |

notations describing the model's elements. We also present the link budget analysis along with the propagation path loss model to estimate the cell ranges. After that, we elaborate on the dimensioning phase where we compute the initial minimum possible number of MRRUs and mRRUs that can satisfy the coverage and capacity constraints. For clarity, we provide the main notations used throughout the paper in Table 1. All the MRRU and mRRU related parameters such as the bandwidth, sub-carrier frequency, and other key parameters are detailed in Table 2 and were based on the 3GPP specifications [38]. It should be noted that changing the system parameters such as the carrier frequency, channel bandwidth, transmit power, etc. will not impact the adopted methodology. However, it will definitely impact the planning output.

### A. SYSTEM PARAMETERS AND LINK BUDGETS

Let $S^i_{\text{RRU}}$ be a set of $i$ type of RRUs in a given geographical area where $i$ is an index representing, MRRUs when $i = \text{UMa}$ and, mRRUs when $i = \text{UMi}$. We denote by $S^i_{\text{RRU}}$ the set of RRUs of type $i$; it can be defined as follows: $S^i_{\text{RRU}} = \{1, 2, \cdots, N^i_{\text{Dim}}\}$ where $N^i_{\text{Dim}}$ denotes the number of RRUs for cell type $i$. The locations of the RRUs along with the UEs' locations are directed in the cartesian plane according to their coordinates $(x, y)$. The locations of RRUs have a dimension up to $N^{\text{UMa}}_{\text{RRU}} + N^{\text{UMi}}_{\text{RRU}}$ that satisfy the planning constraints. We assume that we aim to serve $U$ UEs in a 2-D area having a surface denoted by $S$ expressed in kilometer-square (km$^2$). The area can be subdivided into $P$ subareas. Each subarea $p$ is characterized by its surface $S_p$ where $\sum_{p=1}^{P} S_p = S$ and a particular probability density function denoted by $D_p(x, y)$. For instance, the density could be a uniform distribution with a given user density per km$^2$ or a normal (Gaussian) distribution corresponding to concentrated users in a hotspot region having its density reduced as we move away from the center. We assume that each MRRU/mRRU is equipped with $N_s$ sector antennas and characterized by a list of parameters including transmit power, thermal noise, antenna gain introduced in Table 3 [39].[1] We assume that we are dealing with a single type of UE (e.g., mobile cell phones) that are characterized by the parameters detailed in Table 4. Other UE types could be easily considered in this study but for tractability and clarity, we limit our analysis for one type of UE. The available spectrum is divided into resource blocks denoted by $RB$ consisting of 12 adjacent subcarriers. The Effective Isotropic Radiating Power (EIRP), also noted as $D$, for MRRUs/mRRUs is calculated as: $D = A - B + C_1$. By analogy, the same applies to a UE where its EIRP is: $D' = A' - B' + C'_1$. The thermal noise ($F$) of the MRRUs/mRRUs is calculated as follows:

$$F[\text{dBm}] = 10\log_{10}(\text{KbT} \times RB \times SQ \times BW \times T), \quad (1)$$

where KbT is the Boltzmann's constant, $RB$ is the number of resource blocks, $SQ$ is the subcarrier quantity, $BW$ is the bandwidth in Hz, and $T$ is the temperature in Kelvin. The thermal noise ($F'$) of the UE is computed using the same expression but with the UE parameters. The received sensitivity of the receiver, which is noted ($L$) in the case of UL, and $L'$ in the case of DL, is calculated using the thermal noise, SINR, and the noise figure where $L = G + H + J$ in UL and consequently, $L' = G' + H' + J'$ in DL. The minimum received power by, MRRU, mRRUs or UE, is then

**TABLE 5.** Propagation parameters.

| | Value |
|---|---|
| **Penetration Loss** | 28 dB |
| **Foliage loss** | 4.34 dB |
| **Body block loss** | 0.0 dB |
| **Interference Margin** | 3.0 dB |
| **Rain/ice, Atmospheric Attenuation:** | 3.45,0.06 dB/Km |
| **Slow fading margin** | 8 dB |

[1] The values of the parameters presented in Tables 2, 3, and 4 are provided as a real-case example that we employed later in the simulation results section. Other values can be considered depending on the employed technology related to the RRUs, NR channels, and network parameters according to the network planner needs.

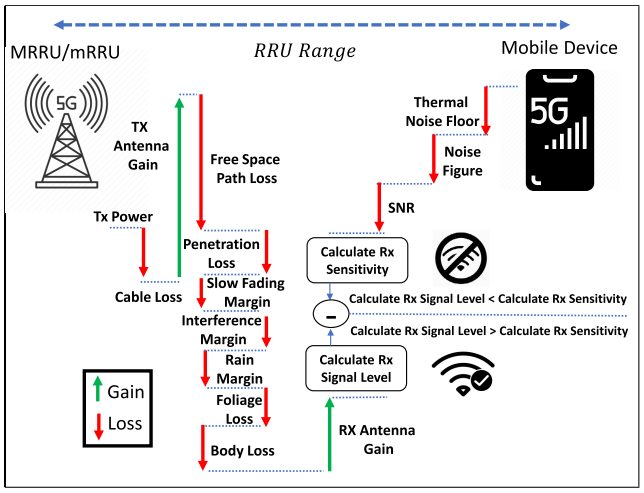


**FIGURE 3.** Illustration of the end-to-end link budget analysis in DL for MRRU/mRUU. The figure highlights the power gains and losses that the signal experiences from the RRU to the UE through the 5G channel.

computed using their received sensitivity, their interference margin, their antenna gain, the mast head amplifier, and their cable loss. Its value for MRRU/mRRU is computed as $L + M - C_2 - N + O$ while for UE is $L' + M' + N' - C_2' + O$.

After computing the minimum received power for MRRUs, mRRUs, and UE, we compute the radio link budget for each cell type $i \in \{\text{UMa,UMi}\}$ to calculate the link performance and estimate the Maximum Allowed Path Loss (MAPL) between the UE and the RRUs for UL and DL directions. The MAPLs represent the maximum energy loss that the signal can experience before reaching the receiver. For both microcell and macrocell analysis, we rely on the 5G New Radio (5G NR) [40], the new radio access technology developed by 3GPP supporting spectrum from 6 GHz to 100 GHz for the 5G. The propagation parameters such as penetration loss, foliage model, and slow fading margin are defined and computed in Table 5. The radio link budgets for MRRU and mRRU in UL and DL are given in Tables 7, 6, 8, 9. We assume that the Time Division Duplex (TDD) is the access scheme for the UL and DL in this study. Frequency Division Duplex (FDD) can still be applied using the corresponding UL/DL frequency bands. An illustration of the budget analysis for the DL direction is illustrated in Fig. 3. It allows the computation of the MAPL for MRRU and mRRU in UL and DL as follows:

$$\begin{aligned}\text{MAPL}_x^i[\text{dB}] = {} & \text{EIRP}_x^i[\text{dBm}] - 10\log_{10}(RB) - (BL)^i[\text{dB}] \\ & - (PL)^i[\text{dB}] - (FL)^i[\text{dB}] - (\text{RIL})^i[\text{dB}] \\ & - (\text{SLF})[\text{dB}] - (RS)_x^i[\text{dB}] - (IM)^i[\text{dB}] \\ & + (AG)_x^i[dBi] + (\text{MHA})_x^i[\text{dB}], \end{aligned} \tag{2}$$

where $BL$, $PL$, $FL$, RIL, SLF, $RS$, $IM$, $AG$, and MHA are the body loss, penetration loss, foliage loss, rain/ice loss, slow fading, receiver sensitivity, interference margin, antenna gain, and mast head amplifier, respectively. The terms $Y^i, i \in \{\text{UMa,UMi}\}$ represent the term $Y$ specific for cell type $i$ and $x$ represents the propagation direction which is either, UL or DL. We note that the term $(\text{RIL})^{\text{UMa}}$ is set to 0 since the effect of rain and ice interference is negligible in sub-6 GHz frequencies.

### B. DIMENSIONING PHASE

The purpose of the dimensioning phase is to estimate beforehand the required number of MRRUs and mRRUs needed to ensure full network coverage over the region of interest and the fulfillment of the users' traffic demand. Ensuring network coverage guarantees that the UE in the area of interest will not be in a "dead spot" region. On the other hand, the fulfilment of the users' traffic demand guarantees a satisfactory QoS for the UE with UL and DL data rates higher than the minimum requirements. The dimensioning phase relies on the UL and DL link budgets presented earlier, the path loss propagation models, and the cell capacities of MRRUs and mRRUs. To this end, we investigate both the coverage dimensioning and cell capacity dimensioning.

#### 1) COVERAGE DIMENSIONING

The numerical results of the link budget analysis that was performed earlier and yielded the MAPL, defined in (2), are included in Tables 6, 7, 8, and 9. As it is showing, the MAPL of MRRU in UL is 140.06 dBm and for DL is 159.06 dBm using the adopted system parameters. On the other hand, the MAPL of mRRU in UL is $113.04 - d_{3D} \times$ RIM dBm and for DL is $120.04 - d_{3D} \times$ RIM dBm where $d_{3D}$ is the 3D distance separating the RRUs and the UEs. Notice that the MAPL for mRRU is a function of $d_{3D}$ because we introduced RIM, the rain/ice margin, which is distance proportional.

The next step in this dimensioning phase consists in finding the radius $R_{\text{RRU}}^i$ of macro and micro cells in such a way that the whole area $S$ can be covered. In order to achieve that, we define an appropriate path loss model. We rely on the GPP 38.901 [41] standard to utilize suitable path loss models, noted as PL. Since mRRUs generally operates on short range while MRUUs act on larger range, we choose to use Non-line-of-sight propagation (NLOS) model for macro cells while line-of-sight propagation (LOS) model for micro cells. Furthermore, the path loss model for NLOS targetting MRRus can be written as follows [41]:

$$PL^{\text{UMa}}[\text{dB}] = \max\left(PL_{\text{UMa-LOS}}, PL'_{\text{UMa-NLOS}}\right) \quad \text{for } 10\text{ m} \le d_{2D} \le 5\text{ km} \tag{3}$$

using

$$PL'_{\text{UMa-NLOS}} = 13.54 + 39.08\log_{10}(d_{3D}) + 20\log_{10}(f_c) - 0.6\,(h_{\text{UE}} - 1.5)\,, \tag{4}$$

$$PL_{\text{UMa-LOS}} \begin{cases} 28.0 + 22\log_{10}(d_{3D}) + 20\log_{10}(f_c^{UMa}), \\ \text{if } 10\text{ m} \le d_{2D} \le d'_{\text{BP}} \\ 28.0 + 40\log_{10}(d_{3D}) + 20\log_{10}(f_c^{UMa}) \\ -9\log_{10}((d'_{\text{BP}})^2 + (h_{\text{RRU}} - h_{\text{UE}})^2), \\ \text{if } d'_{\text{BP}} \le d_{2D} \le 5\text{ km}, \end{cases} \tag{5}$$

where $d'_{\text{BP}}$ denotes the break-point distance, $f_c$ is the centre frequency in GHz, $h_{BS}$ and $h_{UT}$ are the antenna heights and

**TABLE 6.** MRRU DL link budget analysis.

| Downlink | Unit | Value |
|---|---|---|
| *Transmitter, MRRU* | | |
| Radiating Power EIRP (D) | dBm | 58 |
| *Receiver, Terminal (UE)* | | |
| Thermal Noise (G) | dBm | -130.7 |
| Noise Figure (H) | dB | 4 |
| Receiver Noise Floor (I) | dBm | -116.4 |
| SINR (J) | dB | -7 |
| SNR (K) | dB | 12 |
| Receiver Sensitivity (L) | dBm | -123.4 |
| Minimum Received Power | dBm | -118.4 |
| Indoor Loss | dB | 0 |
| **MAPL (Downlink)** | **dB** | **159.06** |

**TABLE 7.** MRRU UL link budget analysis.

| Uplink | Unit | Value |
|---|---|---|
| *Transmitter, Terminal (UE)* | | |
| Radiating Power EIRP (D') | dBm | 24 |
| *Receiver, MRRU* | | |
| Thermal Noise (G') | dBm | -104.4 |
| Noise Figure (I') | dB | 2 |
| Receiver Noise Floor (J') | dBm | -116.4 |
| SINR (K') | dB | -7 |
| Receiver Sensitivity (L') | dBm | -107 |
| Minimum Received Power | dBm | -120.4 |
| Indoor Loss | dB | 0 |
| **MAPL (Downlink)** | **dB** | **140.06** |

**TABLE 8.** mRRU DL link budget analysis.

| Downlink | Unit | Value |
|---|---|---|
| *Transmitter, mRRU* | | |
| Radiating Power EIRP (D) | dBm | 40 |
| *Receiver, Terminal (UE)* | | |
| Thermal Noise (G) | dBm | -123.9 |
| Noise Figure (H) | dB | 11 |
| Receiver Noise Floor (I) | dBm | -107.2 |
| SINR (J) | dB | -2 |
| SNR (K) | dB | 34 |
| Receiver Sensitivity (L) | dBm | -90.2 |
| Minimum Received Power | dBm | -106.38 |
| Indoor Loss | dB | 0 |
| **MAPL (Downlink)** | **dB** | **120.04-$d_{3D}$ × RIM** |

**TABLE 9.** mRRU UL link budget analysis.

| Uplink | Unit | Value |
|---|---|---|
| *Transmitter, Terminal (UE)* | | |
| Radiating Power EIRP (D') | dBm | 24 |
| *Receiver, mRRU* | | |
| Thermal Noise (G') | dBm | -130.7 |
| Noise Figure (I') | dB | 4 |
| Receiver Noise Floor (J') | dBm | -116.4 |
| SINR (K') | dB | -7 |
| Receiver Sensitivity (L') | dBm | -133.7 |
| Minimum Received Power | dBm | -114.38 |
| Indoor Loss | dB | 0 |
| **MAPL (Downlink)** | **dB** | **113.04-$d_{3D}$ × RIM** |

user height, respectively, $d_{2D}$ is the 2-D distance between the UE and RRU in meters, and $d_{3D}$ is the 3-D distance in meters calculated as: $d_{3D} = \sqrt{d_{2D}^2 + (h_{RRU} - h_{UE})^2}$.

The path loss model for mRRUs in LOS is written as [41]:

$$PL^{\text{UMi}}[\text{dB}] = \begin{cases} 32.4 + 21\log_{10}(d_{3D}) + 20\log_{10}(f_c^{UMi}), \\ \text{if } 10\text{ m} \le d_{2D} \le d'_{BP} \\ 32.4 + 40\log_{10}(d_{3D}) + 20\log_{10}(f_c^{UMi}) \\ -9.5\log_{10}((d'_{BP})^2 + (h_{RRU} - h_{UT})^2), \\ \text{if } d'_{BP} \le d_{2D} \le 5\text{ km}. \end{cases} \quad (6)$$

Consequently, the cell range for cell type $i$ in $x$ propagation direction is $\text{RBS}_x^i = \{d \in \mathcal{R}^+ \text{ where } PL^i(d) = \text{MAPL}_x^i\}$. Once the ranges are determined for UL and DL, the cell radius $\text{RBS}^i$, for cell type $i$ is $\text{RBS}^i = \min(\text{RBS}_{UL}^i, \text{RBS}_{DL}^i)$. Eventually, the number of MRRUs and mRRUs needed to cover the area of interest is expressed as follows:

$$N_{\text{Cov}}^i = \left\lceil \frac{S}{S_{\text{Cell}}^i} \right\rceil, \quad (7)$$

where the symbol $\lceil . \rceil$ denotes the ceiling function and $S_{cell}^i$ is the surface of the cell with radius $\text{RBS}^i$. For instance, $S_{Cell}^i = \pi \times (\text{RBS}^i)^2$ for a circular cell and $S_{Cell}^i = \frac{3\sqrt{3}}{2}(\text{RBS}^i)^2$ for a hexagonal cell.

### 2) CELL CAPACITY DIMENSIONING

In the cell capacity dimensioning, we estimate at first the maximum number of users $N_U^i$ for $i \in \{\text{UMa,UMi}\}$ that can be served simultaneously by one MRRU or mRRU, respectively. The objective is to find the number of RRUs $N_{\text{Cap}}^i$ required to satisfy the DL data rate for a type $i$ cell. Let $SE_{DL}^i$ and $SE_{UL}^i$ be the spectral efficiency of cell $i$ in the DL. It can be determined based on the specifications of the transmitter and receiver [42]. We define $C_s^i$ as the capacity of cell $i$ per sector antenna $s$. $C_s^i$ corresponds to the maximum data rate that will be shared between all UEs connected to the sector antenna $s$ of a cell of a type $i$. Its value is computed as $C_s^i = BW^i \times SE^i$ where $BW^i$ is the channel bandwidth in Hz while $SE^i$ is the spectral efficiency in bits/s/Hz of a type $i$ cell. For instance, for a cell type $i$ in DL using $SQ = 1204$ kHz, TDD, 1 layers of MIMO, and 64 QAM modulation,

the spectral efficiency is 138.6 bits/s/Hz. We assume that users have a target data rate that they aim to achieve in DL, denoted by $T_{DR}(DL)$. Thus, $N_U^i$ can be expressed as follows:

$$N_U^i = \left\lceil \frac{N_s \times C_s^i}{T_{DR}(DL)} \right\rceil. \tag{8}$$

For each subarea $p$, the estimated number of RRUs of type $i$, denoted by $N_{Cap_p}^i$, can be then computed as follows:

$$N_{\text{Cap}_p}^i = \frac{U \iint_{S_p} D_p(x,y)dxdy}{N_U^i}. \tag{9}$$

Consequently, the total number of RRUs of type $i$ in the whole area $S$ is:

$$N_{\text{Cap}}^i = \sum_{p=1}^{N_{Area}} N_{\text{Cap}_p}^i. \tag{10}$$

Finally, the estimated initial number of RRUs $N_{\text{Dim}}^i$ for each cell type $i \in$ {UMa,UMi} needed to cover the whole area and satisfy the data rate requirement in each subarea is given as follows:

$$N_{\text{Dim}}^i = \max(N_{\text{Cov}}^i, N_{\text{Cap}}^i). \tag{11}$$

## V. PROBLEM FORMULATION

In this section, we formulate the network planning optimization problem that yields a minimum number of MRRUs and mRRUs while simultaneously considering the coverage and cell capacity constraints. The goal is to ensure the fulfillment of the expected data rate requirements and cope with coverage outages. To do so, we propose to simultaneously place MRRUs and mRRUs in a manner that allows each user in the service area to communicate with at least one of these MRRUs/mRRUs while meeting the expected QoS. We aim to find the locations of these RRUs described by a set of 2-tuple vectors, $\{x_j^i, x_j^i\}$ where $j = 1, \ldots, N_{\text{Dim}}^i$ and $i \in$ {UMa, UMi} that satisfy the planning constraints. At first, we start by defining the system's decision variables and constraints. After that, we formulate our objective function and propose the optimization problem.

### A. DECISION VARIABLES AND CONSTRAINTS

In this problem, we distinguish two decision variables: i) the tuplet $(x_j^i, y_j^i)$, $\forall j, \forall i$, which are the continuous variables indicating the 2D location of the placed RRUs and ii) a binary variable, denoted by $\rho_j^i$, indicating whether RRU $j$ of type $i$ is ultimately installed or not. Indeed, after some RRUs can be eliminated after simultaneously placing all the nodes due to cell overlaps.

#### 1) COVERAGE CONSTRAINT

Let $N_{\text{PoI}}$ be the number Points of Interest (PoI) that are distributed uniformly over the area of interest $S$. We consider that the whole area is covered only if all $N_{\text{PoI}}$ points are covered. A PoI $n$ in a position $(x_n, y_n)$ is covered if is located within the range of at least one of the deployed MRRUs/mRRUs. The precision of the problems solution increases by increasing the value of $N_{\text{PoI}}$. However, the complexity of the problem also increases leading to higher running time. To denote the state of a PoI $n$, we introduce the binary indicator $\lambda_n$, where $n \in \{1, \cdots, N_{\text{PoI}}\}$, as follows:

$$\lambda_n(x_n, y_n) = \begin{cases} 1, & \text{if PoI } n \text{ is covered by at least one RRU,} \\ 0, & \text{otherwise.} \end{cases} \tag{12}$$

The value that takes $\lambda_n$ depends on the locations $\{x_j^i, y_j^i\}$ of the RRUs. Hence, to ensure the full coverage of the area of interest, the following constraint has to be satisfied:

$$\sum_{n=1}^{N_{\text{PoI}}} \lambda_n(x_n, y_n) \geq \theta N_{\text{PoI}}, \tag{13}$$

where $\theta \to 1$ is a tolerance factor added to relax the coverage constraint.

#### 2) CELL CAPACITY CONSTRAINT PER SUBAREA

To ensure satisfactory QoS, we need to guarantee that each subarea has sufficient RRUs to serve UEs with the minimum required data rate. To this end, we associate to each triplet (sector $s$, subarea $p$, RRU $j$) the continuous parameter $\eta_{s,p,j}$, where $(0 \leq \eta_{s,p,j} \leq 1, \forall s \in \{1, \cdots, N_s\}, \forall p \in \{1, \cdots, P\}, \forall j \in S_{\text{RRU}}^i$, and$\forall i \in$ {UMa, UMi} to measure the presence of RRU $j$ in subarea $p$ if located at position $(x_j^i, y_j^i)$ as follows:

$$\eta_{s,p,j}(x_j^i, y_j^i) = \frac{a_{s,p,j}(x_j^i, y_j^i)}{S_p}, \tag{14}$$

where $a_{s,p,j}(x_j^i, y_j^i)$ is the portion of surface resulting from the intersection of the sector $s$ of RRU $j$ of type $i$ having as coordinates $(x_j^i, y_j^i)$ and the subarea $p$ in km$^2$. Hence, the effective number of UEs in subarea $p$ that are covered by sector $s$ of RRU $j$ of type $i$ can be expressed as follows:

$$N_{s,p,j}^{\text{Cov}} = \eta_{s,p,j}(x^i y_j^i) \times U \iint_{S_p} D_p(x,y)\, dxdy, \tag{15}$$

and the effective number of UEs the whole area that are covered by sector $s$ of RRU $j$ of type $i$ can be expressed as follows:

$$N_{s,j}^{\text{Cov}} = \sum_{p=1}^{P} N_{s,p,j}^{\text{Cov}}. \tag{16}$$

Consequently, to respect the cell capacity of each sector $s$ of cell $j$ of type $i$ (i.e., $\frac{N_U^i}{N_s}$), we compute the number of UEs that are effectively served by each sector in subarea $p$ as follows:

$$N_{s,p,j}^{\text{Ser}} = \begin{cases} \lfloor N_{s,p,j}^{\text{Cov}} \rceil & \text{if } N_{s,j}^{\text{Cov}} \leq \frac{N_U^i}{N_s}, \\ \lfloor \frac{N_{s,p,j}^{\text{Cov}} N_U^i}{N_{s,j}^{\text{Cov}} N_s} \rceil & \text{if } N_{s,j}^{\text{Cov}} > \frac{N_U^i}{N_s}, \end{cases} \tag{17}$$

where $\lfloor . \rceil$ denotes the rounding to the nearest integer function.

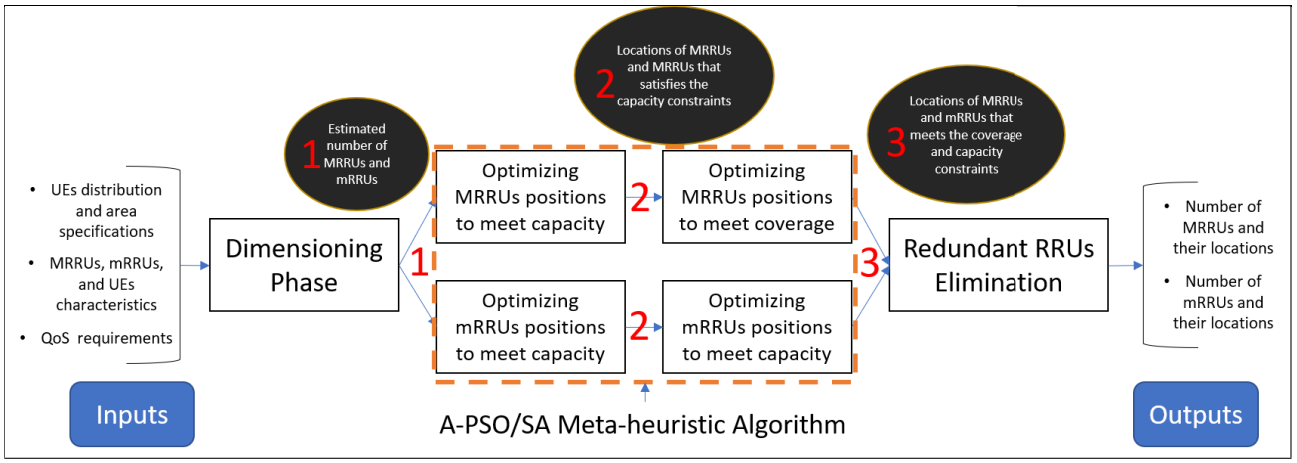


**FIGURE 4.** Proposed approach to solve the planning problem for MRRUs and mRRUs placement using meta-heuristics.

Finally, to ensure that all UEs' QoS is satisfied, the following condition has to be satisfied:

$$\sum_{i\in\{\text{UMa,UMi}\}}\sum_{j=1}^{N^i}\sum_{s=1}^{S} N_{s,p,j}^{\text{Ser}} \geq \mu\, U \iint_{S_p} D_p(x,y)\,dxdy, \quad \forall p = 1,\cdots,P, \tag{18}$$

where $\mu \rightarrow 1$ is a tolerance parameter added to relax the cell capacity constraint.

### B. OPTIMIZATION PROBLEM

The overall optimization problem for a heterogeneous network planning can be written as follows:

$$\text{(P)}: \underset{\rho_j^i\in\{0,1\},(x_j^i,y_j^i)\in S\times S}{\text{minimize}} \sum_{i\in\{\text{UMa,UMi}\}}\sum_{i=1}^{N_{\text{Dim}}^i} \rho_j^i, \tag{19}$$

Subject to:

$$\sum_{i\in\{\text{UMa,UMi}\}}\sum_{j=1}^{N_{\text{Dim}}^i}\sum_{s=1}^{S} N_{s,p,j}^{\text{Ser}} \geq \mu\, U \iint_{S_p} D_p(x,y)\,dxdy, \quad \forall p = 1,\cdots,P \tag{20}$$

$$\sum_{n=1}^{N_{\text{PoI}}} \lambda_n(x_n,y_n) \geq \theta N_{\text{PoI}}. \tag{21}$$

Note that the values $\lambda_n$ and $N_{s,p,j}^{\text{Ser}}$ depend directly on the RRUs locations (i.e., $(x_j^i, y_j^i)$). The optimization problem (P) is NP-hard which is computationally expensive to solve. Therefore, in the following section, we introduce a two-step process where, in its first phase, we utilize meta-heuristic optimization algorithm to determine the locations of RRUs separately and then we proceed by a RRU elimination phase to remove redundant units.

## VI. META-HEURISTIC PLANNING APPROACH

In this section, we present a heuristic approach that solves the 5G network planning problem while aiming to minimize the objective function of the optimization problem (P) without violating its constraints. As Fig. 4 shows, the process solves the optimization problem in two steps. First, the MRRUs/mRRUs are placed separately while optimizing their locations $(x_j^i, y_j^i)$ by exploiting the random behavior the algorithms. Then, all the RRUs are placed at the same time and we eliminate eventual redundant MRRUs/mRRUs by dealing with the binary vector $\rho_j^i$.

### A. RRU PLACEMENT USING A-PSO

In the recent years, PSO has become a better developed optimization algorithm by searching the optimal solution through continuous iterations and employing the size of the value of the objective function. A-PSO [43], an enhanced version of PSO, enables faster convergence and has been successfully applied to many classes of problems, such as mechanical, and structural optimization, and multi-objective optimization, artificial neural network training, and fuzzy system control. These advantages have classified A-PSO as the best approach and motivated researchers to more rely on A-PSO. Moreover, the reason behind choosing A-PSO among other heuristics is: (i) its search processes is simple and easy to implement by manipulating few numerical parameters (e.g., such as the number of particles, inertial weights, and acceleration factors), (ii) it require low computational cost attained from small number of agents, and finally, (iii) it provides a good convergence speed. Moreover, A-PSO has more advantages in contrast to other algorithms such as Genetic Algorithms (GA), and Tabu search which are used for a finite number of optimization combinations. A-PSO can deal with an infinite set of MRRUs/mRRUs with an easy implementation. Compared to other evolutionary computation techniques such as GA, A-PSO is a more simple concept that have few parameters to adjust, robustness to control parameters, and a faster convergence while yielding better results in most cases. It deals with continuous values and takes real numbers as particles.

**Algorithm 1:** A-PSO Algorithm for MRRUs and mRRUs Deployment

Generate an initial Swarm Population $SP$ composed of $k$ random particles $Z^{(k)}$, with $k = 1, 2, \ldots, K$ and size $2N^{i}_{\text{Dim}} \times 1$.
$Q_1^{\min} = 0$, $h = 0$ and set $Q = Q_2$.
**while** $Q_1^{\min} < \theta N_{PoI}$ **do**
  **for** $k = 1, 2, \ldots, K$ **do**
    Evaluate $Q^{(k)}(h), \forall k = 1, 2, \ldots, K$.
  **end**
  **if** $\arg\min_{k,h} Q^{(k)}(h) \neq 0$ **then**
    Find $(k_m, h_m) = arg_{k,h} \min Q^{(k)}(h)$, with $k_m$ the index and $h_m$ the location of the particle $k$ which is the output of the lowest utility $Q$.
    Set $Q^{\min} = Q^{k_m}(h_m)$ and $Z^G = Z^{k_m}(h_m)$.
    Find $h_{h_k} = \arg\min_{k,h} Q^{(k)}(h)$ for each $k$ where $h_{h_k}$ expresses the position of $k$ which is the output of the lowest utility.
    Set $Q^{(I,h_k)} = Q^{(k)}(h_{h_k})$ and $Z^{(I,h_k)} = Z^{(k)}(h_k)$.
    Regulate the velocity and the position of all particles based on equations (24) and (25) respectively.
  **else**
    $Q = Q_1$ which is shifting the utility $Q$ to $Q_1$.
  **end**
  $h = h + 1$.
**end**

The principle of A-PSO is to let the particle migrate towards the best location in search space and remember each particle's best-known location and global (swarm) best-known location. Each particle preserves the path of its best solution, which is the personal best (noted as *pbest*), and the global best (noted as *gbest*). The A-PSO solves the optimization problem by dividing it in 4 steps: i) At first, it initialize swarm in hyperspace, ii) then, it estimate the fitness of individual particles, iii) after that, it adjust velocities based on preceding best and global (or neighborhood) best states, and finally iv) it finishes some conditions or return to step ii). The particle represents the candidate solution, and the number of candidate solutions constitutes the swarm called population.

We generate $K$ number of particles $Z^k, k = 1, 2, \ldots, K$ of $2N^{i}_{\text{Dim}} \times 1$, where $i \in \{\text{UMa, UMi}\}$ dimensions in the initial swarm Generation. Initially, the vector $Z^{(k)} = [x^{(k)}, y^{(k)}]$ contains the random positions of either MRRUs or mRRUs in the region of interest. Then, A-PSO calculates the next two utilities functions $Q_1^{(k)}$ and $Q_2^{(k)}$ realized by each particle $k$. They are defined as follows:

$$Q_1^{(k)} = \begin{cases} -\sum_{n=1}^{N_{\text{PoI}}} \lambda_n^k & \text{if (18) is satisfied by k particles,} \\ 0, & \text{otherwise,} \end{cases} \tag{22}$$

$$Q_2^{(k)} = -\sum_{p=1}^{P} \Big| \sum_{i \in \{\text{UMa,UMi}\}} \sum_{j=1}^{N^{i}_{\text{Dim}}} \sum_{s=1}^{S} N^{\text{Ser}}_{s,p,j} - \mu\, U \iint_{S_p} D_p(x, y)\, dxdy \Big|. \tag{23}$$

$Q_1^{(k)}$ in equation (22) represents the number of points of interest covered by MRRUs/mRRUs. It is set to 0 if the cell capacity constraints expressed in equation (18) is not satisfied for at least one subarea. If this is the case, we assume that the particle $k$ does not cover the region at all. $Q_2^{(k)}$ in equation (23) is used to calculate the difference between the minimum required number of users that have to be served and the number of users served by particle $k$.

If all particles failed to satisfy constraint (18), the A-PSO aims then to minimize the utility to $Q_2^{(k)}$ until it finds a feasible solution. Once that is done, it switches back to utility $Q_1^{(k)}$ attempting to minimize it until reaching $-\theta N_{\text{PoI}}$. At each iteration, A-PSO calculates the global particle denoted by $Z^G$, that offers the best utility (i.e., either $Q_1$ or $Q_2$ depending on the feasibility of the particles in this iteration). Moreover, the activities of the particles are directed by their own best-known location in the search space and the entire population's best-known location. Therefore, A-PSO keeps the record of the position based on the best performance for each iteration $k$ represented $Z^{(k,\text{G})}$, and computes and updates the velocity $V_v^{(k)}, \forall v = 1, \cdots, 2 \times N^{i}_{\text{RRU}}$ of each iteration $h$ and the position of each element $V_v$ are obtained by the following equations:

$$V_v^{(k)}(h+1) = V_v^{(k)}(h) + c_1 r_n + c_2 \left( Z_v^{(K,\text{G})}(h) - Z_v^{(k)}(h) \right), \tag{24}$$

where $r_n$ is drawn from $N(0, 1)$ to replace the second term. The update of the position is performed as follows:

$$Z_v^{(k)}(h+1) = Z_v^{(k)}(h) + V_v^{(k)}(h+1) \tag{25}$$

In the above equation, the parameters $c_1$ and $c_2$ are positive and called "acceleration coefficients", the values of $c_1$ and $c_2$ are close to 1 ($c_1 + c_2 = 1$ is empirically selected value). The A-PSO updates each element $v$ of a particle $Z^{(k)}$ using equation 25. The restricted value of velocity called $V_max$ is used if the velocity exceeds the prefixed limit. A-PSO performance is conditioned on the values of parameters, and the optimal values of parameters depend on the problem at hand. The process is reproduced, and by doing so, it is expected to reach the convergence either by succeeding the maximum number of iterations or by achieving the algorithm objective (i.e., $Q_1 \leq -\theta N_{\text{PoI}}$). Lastly, the optimized solution is given by $Z_{\text{opt}} = Z^G$. Note that convergence does not guarantee that a reasonable solution will eventually be founded in theory. The target $Q_1$ cannot be reached unless the cell capacity constraint is satisfied which is the case thanks to the introduction of $Q_2$. The solution is performed with the guaranteed convergence A-PSO in which particles perform a random search *gbest*, and the performance is enhanced in the

problems under attention. Algorithm 1 optimizes the number and the locations of MRRUs and mRRUs in the system.

### B. RRU PLACEMENT USING SA

Simulated annealing exploits an analogy between the way in which a metal cools and freezes into a minimum energy crystalline structure (the annealing process) and the search for a minimum in a more general system. The algorithm is based upon the one presented in [44], which was originally proposed as a means of finding the equilibrium configuration of a collection of atoms at a given temperature. The algorithm employs a random search by applying arbitrarily perturbation on the parameters of the objective function. And as the algorithm is moving from one state to another, not only does it keep all the perturbations that decrease, but also it accepts the perturbations that increase it with a probability $p$.

In our case, the implementation of SA to optimize RRUs placement in a 5G network is described as follows; First, we initialize locations of RRUs by placing them on a rectangular grid. After that, we select randomly an RRU and we move its position by randomly modifying its $(x_j^i, y_j^i)$, $\forall j, \forall i$, coordinates to $(x_j^i + \Delta x, y_j^i + \Delta y)$, where $\Delta x$ and $\Delta y$ are random perturbations. We then associate the users to RRUs after moving the selected RRU to its new position. We perform resource allocation and calculate the interference and data rates and also compute the percentage of users in outage. If the outage rate decreased compared to the previous iteration, we accept the new result, and update the SA temperature $T_{n+1} = c \times T_n$, with $(0 \leq c \leq 1)$. Otherwise, we accept the result with a probability $e^{\frac{-\text{NewResult}-\text{OldResult}}{T}}$. The objective is to occasionally accept values that increase the objective function (here the outage rate) in order to avoid being trapped in local minima. This process is repeated until a certain number of values is accepted or until a maximum number of iterations is reached. The number of accepted values and the maximum number of iterations are set proportionally to the number of RRUs. Hence the algorithm has polynomial complexity in the number of RRUs.

### C. ELIMINATION OF REDUNDANT MACRO AND MICRO RRUs

After separately determining the locations of the MRRUs and mRRUs using the A-PSO or SA algorithms, Algorithm 2 removes redundant MRRUs and mRRUs in the proposed model based on consecutive elimination one at a time. We assume that all RRUs are located in the region of interest. The elimination process is repeated as follows: First, the MRRUs and mRRUs are placed in the area of interest using one of the meta-heuristics algorithms. Then, we simulate the removal of each RRU one by one and compute the effect of the action on the network (i.e., coverage and QoS). Finally, the RRUs that do not deteriorate the network are considered redundant and therefore removed. Given a combined set of MRRUs and mRRUs denoted by $\epsilon$ and divided into two subsets $\epsilon_1$ and $\epsilon_2$. MRRUs or mRRUs in $\epsilon_1$ are considered redundant and can be eliminated without affecting the equations (13) and (18) while any elimination of RRUs in $\epsilon_2$ affects the problem solution and are considered indispensable. The objective is to keep all RRUs in $\epsilon_2$ and eliminate the RRUs in $\epsilon_1$ to reach the optimized locations of MRRUs and mRRUs without causing any service deterioration. We eliminate RRUs one by one while checking continuously whether the equations (13) and (18) remain satisfied or not. If a RRU $f$ affects the equations (13) and (18), it cannot be eliminated and placed into $\epsilon_2$, and its corresponding $\rho_f$ remains 1 else, it is assumed to be removed and placed into set $\epsilon_1$. The algorithm focuses on the set $\epsilon_1$ to determine all RRUs that can be securely eliminated and set their corresponding $\rho_{(f)}$ to 0. If two or more RRUs in $\epsilon_2$ can reinforce each other to keep up the equations (13) and (18), only one that has insignificant influence on the served user denoted by $b$ can be removed. The expression of $b$ is given in algorithm 2. The steps are repeated until reaching to a state that eliminating any of the available RRUs affects the optimization solution.

**Algorithm 2:** Mechanism for Redundant mRRUs and MRRUs Elimination

$h = 0$,
Assume all MRRUs and mRRUs are activated $\rho^i(h) = \{1, \ldots, 1\}$ and $\epsilon$ is the set of all positioned RRUs.
**repeat**
  **for** $f = 1, \ldots, N_{RRU}^{UMa} + N_{RRU}^{UMi}$ **do**
    Remove MRRU/mRRU $f \in \epsilon$ and define $\rho_{(f)}^i(h)$ which corresponding to $\rho^i(h)$ with 0 in the $f^{th}$ position.
  **end**
  **if** *equations* (18) *and* (13) *are still satisfied* **then**
    MRRU/mRRU $f$ can be removed, $f \in \epsilon$.
  **else**
    MRRU/mRRU cannot be removed.
  **end**
  Find MRRU/mRRU $b$ such that:
  $b = argmax_{f \in \epsilon} \sum_{i \in \{\text{UMa,UMi}\}} \sum_{j=1}^{N_{\text{Dim}}^i l} \sum_{s=1}^{S} N_{s,p,j}^{Ser}(Z_{\text{opt}}) - \mu\, U \iint_{S_p} D_p(x, y)\, dxdy$,
  RRU $b$ is totally and carefully removed.
  $\epsilon = \epsilon \setminus b$
  $\rho(h+1) = \rho^i(h)$.
  $h = h + 1$.
**until** $\epsilon = \{\}$;
The final MRRU/mRRU combination after network planning is $\rho^i(h)$.

## VII. EXPERIMENTS AND EVALUATION

In this section, we evaluate the performance of the proposed radio network planning approach for different scenarios. Also, we perform experiments to compare the performances

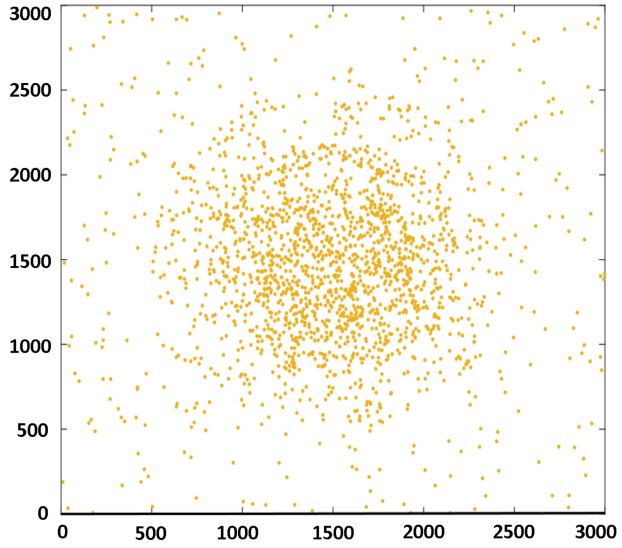


**(a)** Scenario I

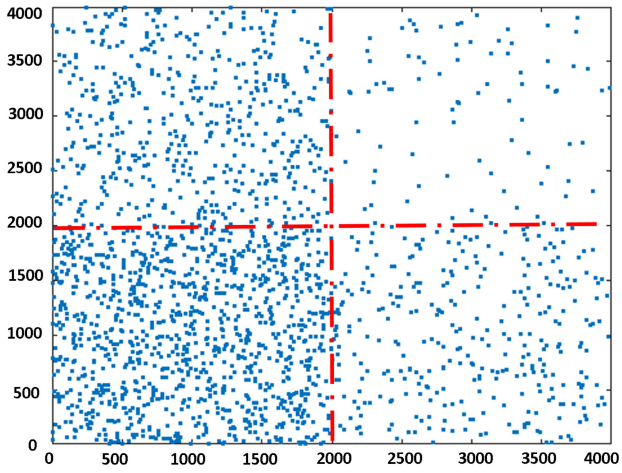


**(b)** Scenario II

**FIGURE 5.** Snapshots illustrating an example of the placement of UEs for (a) Scenario I and (b) Scenario II.

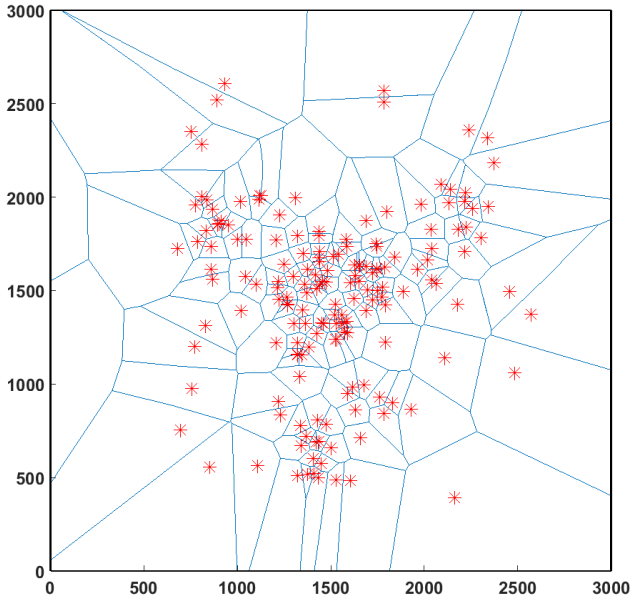


**FIGURE 6.** Voronoi diagram of the 5G Network planning using A-PSO for Scenario I with MRRUs represented by "*" shapes.

of the A-PSO with those obtained by SA for two different UE distribution scenarios.

### A. EXPERIMENTAL SETUP

All simulations were run on MATLAB (R2020a) software performing on a server with a 32 socket Intel(R) Xeon (R) E5-2698 v3 @2.30GHz CPU and 72G of RAM. We propose to conduct experiments on different scenarios where we vary different parameters such as, the number of users and their distribution, the area size, and the number of subareas, etc. These scenarios are presented as follows:

- Scenario I: For this scenario, we target to serve 4000 UEs in a 3 km $\times$ 3 km geographical area. The latter is divided into two sub-areas. As the example in Fig. 5(a) shows, one of the sub-areas is in the form of a 1 km radius circle centered at the center of the map. In this circular area, 60% of the UEs are normally distributed. This subarea corresponds to a dense area where users are concentrated in the center of the region. The rest of UEs are uniformly distributed in the external subarea.
- Scenario II: In this scenario, the number of active UEs is 4000 distributed in four equally sized square subareas. Each square has a surface of 4 km$^2$. The total area is 4 km $\times$ 4 km. The subareas 1, 2, 3, and 4 have 55%, 25%, 15%, and 5% as UE densities, respectively. This is illustrated in Fig. 5(b).

In all of the scenarios, the cell capacity tolerance $\theta$ and the coverage tolerance $\mu$ are set to 97% and 99%, respectively. Based on the selected parameters of UMa, UMi, and UEs included in Table 3, 4, and 5, The computed MRRUs' and mRRUs' total throughput per cell resulting due to the cell capacity dimensioning are 422 Mbps and 1500 Mbps for a spectral efficiency of 21 bps/Hz and 15 bps/Hz, respectively. Our target data rate per UE for this 5G architecture is 50 Mbps, which means that the average number of UEs that can be served simultaneously, per sector, is 8 for MRRUs and 30 for mRRUs. Moreover, the resultant cell range due to the coverage dimensioning is $\text{RBS}^{\text{UMa}} = 1.04$ km for MRRUs while it is $\text{RBS}^{\text{UMi}} = 318.07$ meters for mRRUs. For both A-PSO and SA, the maximum number of iterations is set to 5000 while the number of search agents for PSO is set to 12. The maximum achieved velocity is defined to 500 meters to restrain the action of MRRUs/mRRUs from iteration to another. All of the achieved large scale performance analysis simulations are conducted using a 100 iteration Monte Carlo run and the average values are taken into consideration.

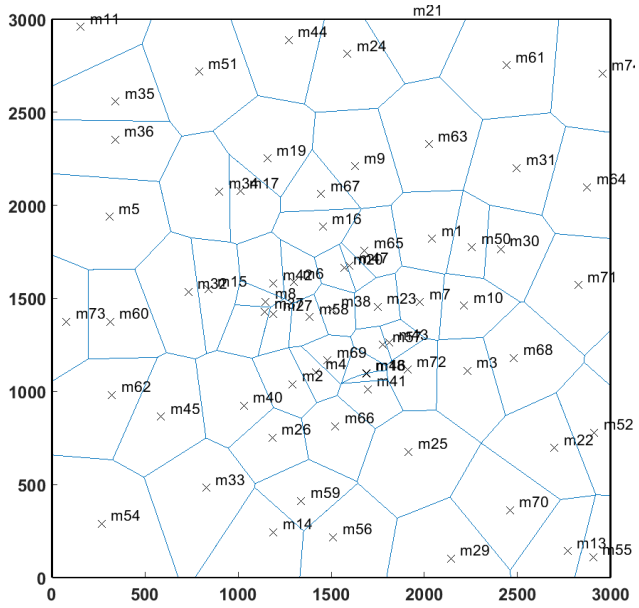


**FIGURE 7.** Voronoi diagram of the 5G Network planning using A-PSO for Scenario I with mRRUs represented by "x" shapes.

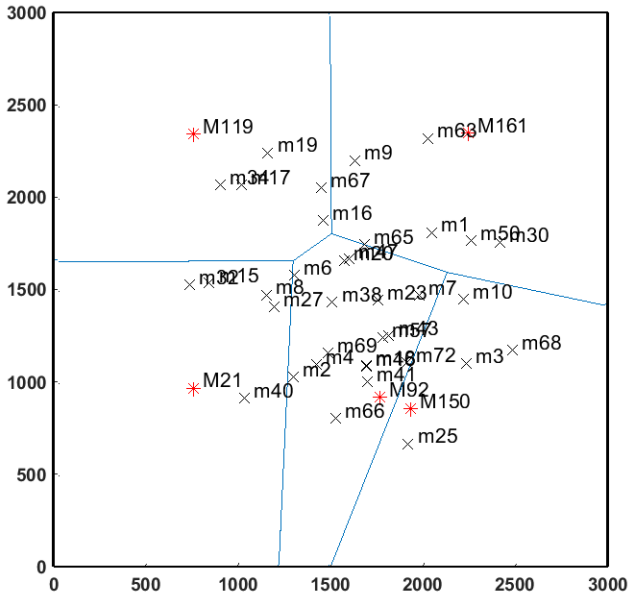


**FIGURE 8.** Voronoi diagram of the 5G Network planning using A-PSO for Scenario I after redundancy elimination with mRRUs and MRRUs represented by "x" shapes and "*" shape, respectively.

### B. SIMULATION RESULTS

For clarity and tractability, we propose to first investigate a small-scale scenario to be able to visualize the different steps of the network planning process. We consider simulating a test case using Scenario I. At first, we start by analyzing a standalone architecture deploying MRRUs and mRRUs using A-PSO to show how the evolutionary algorithm reaches a suboptimal solution for both architectures. After that, we consider a two-tier heterogeneous architecture where we jointly deploy MRRUs and mRRUs using both SA or A-PSO and perform an RRU redundancy elimination. Fig. 6 shows the

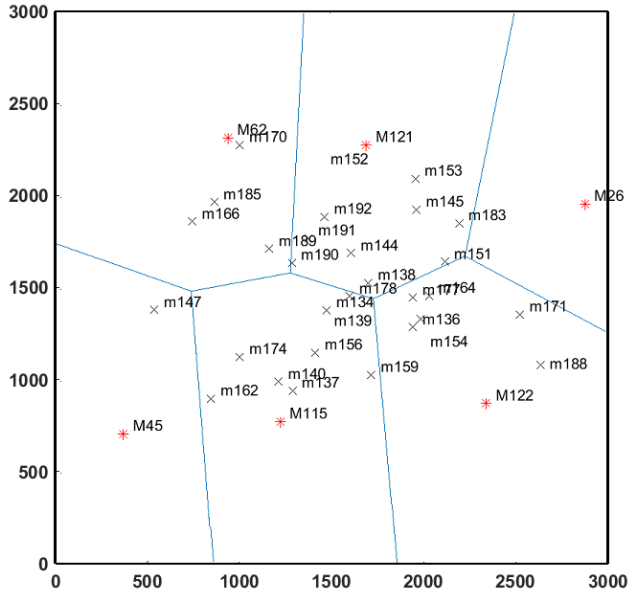


**FIGURE 9.** Voronoi diagram of the 5G Network planning using SA for Scenario I after redundancy elimination with mRRUs and MRRUs represented by "x" shapes and "*" shapes, respectively.

result of a standalone planning for MRRUs while Fig. 7 illustrates a standalone planning of mRRUs, both for Scenario I. The result of the final network planning after redundancy removal for A-PSO is depicted in Fig. 8. We can notice that by placing MRRUs only there is a huge number of base stations placed around the center of the hot spot area in order to satisfy the UEs demand. Large MRRUs with partially extended coverage are placed in the external subarea. In total, 90 MRRUs is needed to satisfy the constraints of problem (P). However, if only mRRUs are placed as shown in Fig. 7, a near-uniform placement of mmWave cells is obtained with a small concentration in the hot spot zone since these cells are characterized by a high capacity. The uniform placement is due to the small coverage achieved by the 50 installed mRRUs. Notice that less mRRUs are required to meet the constraints of problem (P). This is due to the fact that cell capacity constraints for each subarea are more impacting the problem than the coverage one. The figures confirm the ability of the proposed approach using evolutionary algorithm in adapting the planning of RRUs according to the network operator's needs.

By combining the earlier solutions and removing redundant RRUs, we can notice the total number of MRRUs and mRRUs is significantly reduced in the final network topology leaving only 5 MRRUs to fulfil the coverage constraint and 27 mRRUs to meet the UE demand in the hot spot area. Only four mRRUs are placed in the external subarea while the rest are placed in the central subarea. This corroborates the fact that the elimination for redundant RRUs is eliminating nodes while taking into account the coverage and cell capacity constraints in each subarea. In Fig. 9, we provide the final architecture using SA after eliminating redundant RRUs. In general, we obtain similar placement behavior,

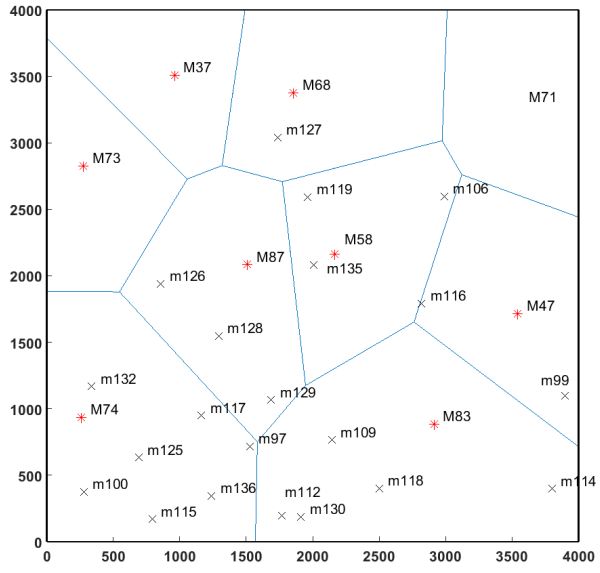


**FIGURE 10.** Voronoi diagram of the 5G Network planning using SA for Scenario II after redundancy elimination with mRRUs and MRRUs represented by "x" shapes and "*" shapes, respectively.

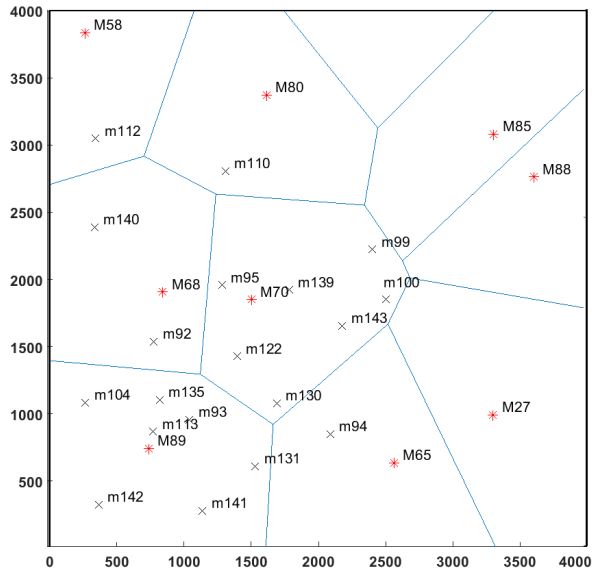


**FIGURE 11.** Voronoi diagram of the 5G Network planning using A-PSO for Scenario II after redundancy elimination with mRRUs and MRRUs represented by "x" shapes and "*" shapes, respectively.

however, with a different number of RRUs. To more illustrate the optimization mechanism for A-PSO and SA, we test the algorithms on Scenario II. We provide the obtained planning illustrated by the resulting Voronoi diagrams using SA and A-PSO in Fig. 11 and Fig. 10, respectively. We notice that, for the two included simulations, the distribution of mRRUs follows the UEs distribution while the MRRUs are essentially used for coverage. Indeed, since the UEs are concentrated in left bottom subarea with a density of 55%, around 11 mRRUs are installed there supported by on average 2 MRRUs (MRRU 74 and two small contributions of MRRU 83 and MRRU

**TABLE 10.** Comparative study between SA and A-PSO after redundancy elimination for $U = 3000$ UEs.

| | | | |
|---|---|---|---|
| SA | Scenario I | Number of MRUUs | 8 |
| | | Number of mRRUs | 25 |
| | | Avg. Coverage Rate | 99.2% |
| | | Avg. Capacity Rate | 99% |
| | Scenario II | Number of MRUUs | 8 |
| | | Number of mRRUs | 20 |
| | | Avg. Coverage Rate | 99.1% |
| | | Avg. Capacity Rate | 98.9% |
| A-PSO | Scenario I | Number of MRUUs | 9 |
| | | Number of mRRUs | 30 |
| | | Avg. Coverage Rate | 99.4% |
| | | Avg. Capacity Rate | 99.9% |
| | Scenario II | Number of MRUUs | 10 |
| | | Number of mRRUs | 17 |
| | | Avg. Coverage Rate | 99.4% |
| | | Avg. Capacity Rate | 99.2 % |

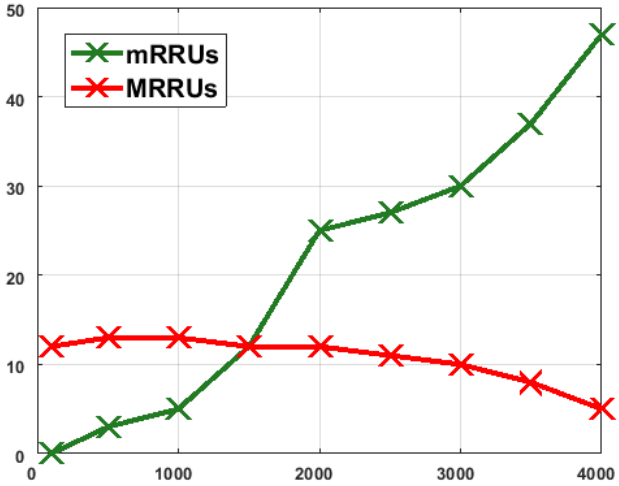


**FIGURE 12.** Variation of the total number of installed RRUs versus the number of UEs using A-PSO for Scenario I.

87 using SA). In the top right subarea where only 5% of UEs exist, only one mRRU is placed to support the existing MRRUs (M71 and parts of M47, M68, and M58 using SA). Similar placement behavior is obtained using A-PSO.

Table 10 provides a summary of the results obtained by both algorithms (A-PSO and SA) with RRU elimination for the two investigated scenarios. We can notice that compared to SA, the A-PSO yields a slightly higher number of RRUs with higher average coverage (more than $\approx 0.4\%$). In general, the algorithms provide very similar performance and behavior.

In Fig. 12, we evaluate the performance of the planning approach by determining the final number of installed MRRUs and mRRUs while varying the number of UEs using the A-PSO algorithm for Scenario I. As we can see,

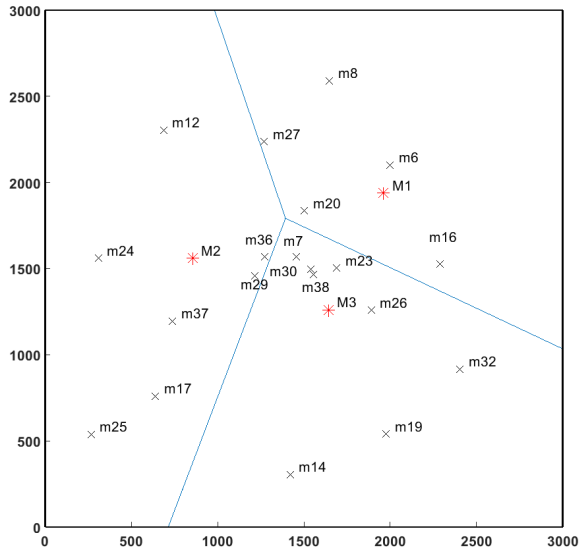


**FIGURE 13.** Voronoi diagram of the 5G Network planning using A-PSO after redundancy elimination with mRRUs (f=28 Ghz and BW=400 MHz) and MRRUs (f=3.5 Ghz and BW=100 MHz) represented by "x" shapes and "*" shapes, respectively.

when increasing the number of UEs, the number of MRRUs slightly decreases while the number of mRRUs significantly increases. This is due to the fact that MRRUs mainly provide coverage and therefore, at a high number of UEs, there is no need to add extra MRRUs. Contrarily, with a high number of UEs, there is a need to provide more bandwidth and hence, increase of mRRUs. The number of MRRUs decreases since the added number of mRRUs can help in compensating the coverage of some MRRUs. On the other hand, when the number of UEs is low ($U = 100$ UEs) no mRRU is needed. These results corroborate the need of applying real-time RRU on/off switching in practice after effectively planning the 5G RAN.

We also perform another experimental simulation where we evaluate the performances of the A-PSO approach followed by the redundant RRU elimination step using other frequency ranges and channel bandwidths for MRRUs and mRRUs. We set the MRRU carrier frequency to the C-Band with 3.5 GHz, instead of 6 GHz, and the channel bandwidth to 100 MHz, instead of 20 MHz. Also, the bandwidth of mRRUs is changed to 400 MHz while keeping the carrier frequency at 28 GHz. It should be noted here by changing the carrier bandwidth to the C-band, the range of MRRUs will increase and by increasing their bandwidth to 100 MHz, MRRUs can serve more UEs simultaneously. Similar remark is noticed for the mRRUs. We set the same number and distribution of users as in Scenario I. The result of this simulation is shown in Fig. 13. We notice that the overall number of deployed RRUs decreases from 32 to 22 as compared to the case illustrated in Fig. 8. The number of mRRUs was importantly reduced and spaced from the center of the area. The decrease in the number of mRRUs can be explained by the increase of the channel bandwidth which results in higher cell capacities and therefore, fewer mRRUs are needed to boost the overall network capacity. The number of MRRUs also decreased to 3 instead of 5 since with the C-Band frequency, MRRUs provide better coverage.

In the next experiment, we evaluate the convergence of the two evolutionary algorithms through the Monte Carlo by observing their convergence rate for each investigated scenario. As Fig. 14 shows, we compute the convergence rate of the two algorithms for MRRUs and mRRUs throughout the iteration run. This is performed for both, the coverage and capacity metrics. The bold red lines represents the capacity satisfaction rate while the bold green line corresponds to the coverage satisfaction rate. The green and red thin lines represents the coverage and capacity tolerances, respectively. Fig. 14(a) and Fig. 14(b) are conducted using the SA while Fig. 14(c) and Fig. 14(d) using A-PSO. We notice that the SA has a faster convergence rate than the A-PSO. Also, the SA often converges from the 10 first iterations for the capacity while PSO achieves this in later iterations. However, for the same number of iterations, we notice that the SA has lower convergence rate than the A-PSO. Notice that for MRRUs, the convergence of the coverage for both SA and A-PSO is achieved at the few first iteration. This is due to the fact that MRRUs have a longer cell range, and therefore, few position adjustment must be made to satisfy capacity. The opposite for mRRUs where capacity constraints are quickly satisfied and adjustment of coverage is needed.

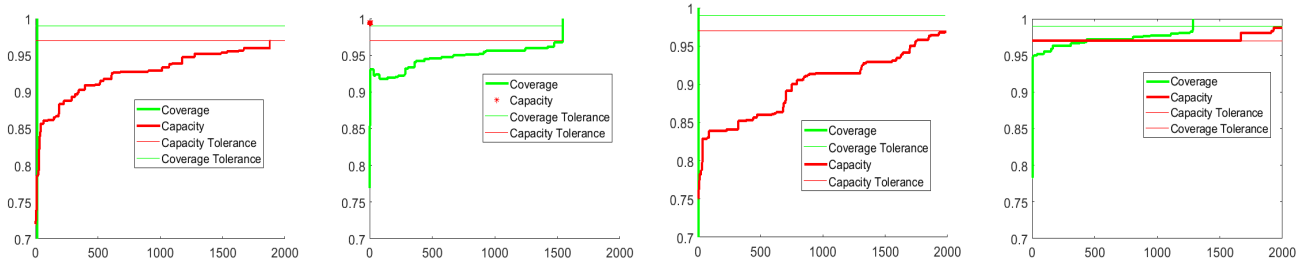


(a) SA for MRRUs (b) SA for mRRUs (c) A-PSO for MRRUs (d) A-PSO for mRRUs

**FIGURE 14.** Convergence rate vs. number of iterations for SA and A-PSO targeting MRRUs and mRRUs for Scenario I. The red line represents the capacity satisfaction while the green line illustrates the coverage satisfaction.

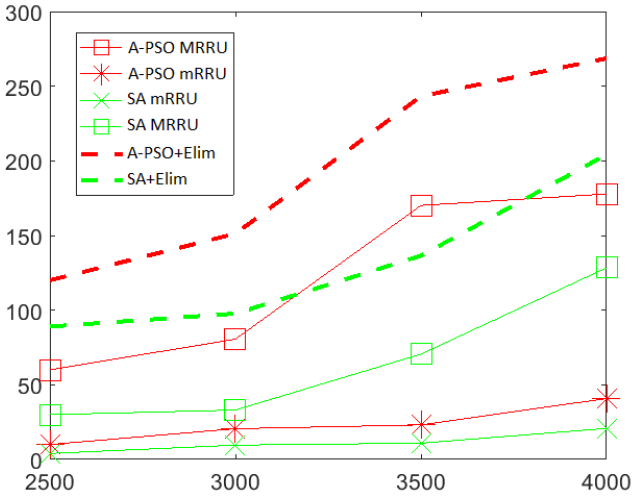


**FIGURE 15.** Running time (s) of the SA and A-PSO, for macro, micro, and after elimination using a size of area 2.5*km* × 2.5*km*, 3*km* × 3 *km*, 3.5*km* × 3.5 *km*, and 4 *km* × 4 *km*.

In order to evaluate the time complexity of the two algorithms: the SA and A-PSO, we perform a running time simulation during which we vary the size of the area of interest in the platform and compute the running time needed for the algorithms to converge to a solution. As Fig. 15 shows, we notice that the A-PSO approach has higher running time than the SA approach for both MRRUs and mRRUs. The time complexity gap increases while increasing the number of size of the area. For both algorithms, the running time while optimization the positions of MRRUs is higher than the one of mRRUs. The two algorithms have a polynomial running time with respect to the area size because the running time increases linearly with the size of the input (i.e., size of the area).

## VIII. CONCLUSION

In this paper, we proposed a 5G planning process for two-tier heterogeneous networks where we deployed microcells, Urban Micro-cells (UMi), broadcasting over mmWave frequencies, on top of a macro-relay network, Urban Macro-cells (UMa), transmitting over the sub-6 GHz frequency band. With suitable link budgets and propagation models, we aimed to optimize and find the locations of the minimum number of possible Macro Remote Radio Units (MRRUs) and Micro Remote Radio Units (mRRUs) to install in an area of interest characterized with different user distributions and densities. In our framework, we start with a dimensioning phase to estimate the number of RRUs to deploy then proceed with a placement phase employing meta-heuristic algorithms that fulfil coverage and user traffic demand constraints. We tested the planning approach using two evolutionary algorithms namely the novel Accelerated Particle Swarm Optimization (A-PSO) and the Simulated Annealing (SA) algorithms. Afterwards, we proceeded with an iterative algorithm to discard redundant RRUs that when eliminated the coverage and cell capacity constraints are not affected. Simulation results using sub-6 GHz UMa and 28 GHz UMi demonstrate that the proposed approach is capable to adapt the placement of the RRUs according to the area characteristics while promoting the placement of mRRUs in dense areas to meet the high throughput demand and employing MRRUs for coverage purposes to maintain connectivity (e.g., less than 2% of outage for the investigated scenarios with almost full coverage). The proposed approach is generic and can be adapted to any scenario. It incorporates the different characteristics and requirements of 5G radio access networks and can be easily extended to multi-tier heterogeneous networks.

The practical deployment of mmWave RRUs is becoming real especially in urban dense areas to meet the increasing traffic demand of the consumers. Although mmWave technology is still requiring LoS links to reach their full throughput potentials, there is tendency to install mmWave nodes in large indoor environments such as shopping malls and airports. Therefore, it is worthwhile to consider the planning of dual-band heterogeneous networks involving sub-6 GHz as well as outdoor/indoor mmWave RRUs. The presented study can be also extended to investigate the green planning by taking into account additional metrics such as the energy consumption of RRUs as well as the limitation of electromagnetic radiation representing one of the major concerns of the 5G cellular networks. Also, designing novel AI approaches leveraging the emerging neural network and deep learning architectures could be a potential future research direction for efficient and rapid planning predicting the required number of RRUs and eventually their placement locations.

## REFERENCES

[1] J. Wang, J. Liu, and N. Kato, "Networking and communications in autonomous driving: A survey," *IEEE Commun. Surveys Tuts.*, vol. 21, no. 2, pp. 1243–1274, 2nd Quart., 2019.

[2] A. Addison, A. Krish, R. Prins, L. Ryan, N. Villette, C. Andrews, N. Azad, D. Bardsley, J. Bauman, J. Diaz, T. Didik, K. Fazliddin, and M. Gromoa, "Low-latency trading in the cloud environment," in *Proc. IEEE Int. Conf. Comput. Sci. Eng. (CSE) IEEE Int. Conf. Embedded Ubiquitous Comput. (EUC)*, Aug. 2019, pp. 272–282.

[3] A. Hamrouni, H. Ghazzai, M. Frikha, and Y. Massoud, "A spatial mobile crowdsourcing framework for event reporting," *IEEE Trans. Comput. Social Syst.*, vol. 7, no. 2, pp. 477–491, Apr. 2020.

[4] G. Zhang and J. Y. B. Lee, "LAPAS: Latency-aware playback-adaptive streaming," in *Proc. IEEE Wireless Commun. Netw. Conf. (WCNC)*, Apr. 2019, pp. 1–6.

[5] S. Yi, S. Chun, Y. Lee, S. Park, and S. Jung, "Overview of LTE and LTE-advanced new features," in *Radio Protocols for LTE and LTE-Advanced*. 2013, pp. 151–158. [Online]. Available: https://ieeexplore.ieee.org/document/8043424, doi: 10.1002/9781118188545.ch7.

[6] H. Althumali and M. Othman, "A survey of random access control techniques for machine-to-machine communications in LTE/LTE—A networks," *IEEE Access*, vol. 6, pp. 74961–74983, 2018.

[7] A. Al-Fuqaha, M. Guizani, M. Mohammadi, M. Aledhari, and M. Ayyash, "Internet of Things: A survey on enabling technologies, protocols, and applications," *IEEE Commun. Surveys Tuts.*, vol. 17, no. 4, pp. 2347–2376, 4th Quart., 2015.

[8] H. Ghazzai, E. Yaacoub, A. Kadri, H. Yanikomeroglu, and M.-S. Alouini, "Next-generation environment-aware cellular networks: Modern green techniques and implementation challenges," *IEEE Access*, vol. 4, pp. 5010–5029, Sep. 2016.

[9] J. G. Andrews, S. Buzzi, W. Choi, S. V. Hanly, A. Lozano, A. C. K. Soong, and J. C. Zhang, "What will 5G be?" *IEEE J. Sel. Areas Commun.*, vol. 32, no. 6, pp. 1065–1082, Jun. 2014.
[10] O. Arouk, T. Turletti, N. Nikaein, and K. Obraczka, "Cost optimization of cloud-RAN planning and provisioning for 5G networks," in *Proc. IEEE Int. Conf. Commun. (ICC)*, Kansas City, MO, USA, May 2018, pp. 1–6.
[11] P. Fan, J. Zhao, and C.-L. I., "5G high mobility wireless communications: Challenges and solutions," *China Commun.*, vol. 13, no. 2, pp. 1–13, 2016.
[12] P. Demestichas, A. Georgakopoulos, K. Tsagkaris, and S. Kotrotsos, "Intelligent 5G networks: Managing 5G WirelessMobile broadband," *IEEE Veh. Technol. Mag.*, vol. 10, no. 3, pp. 41–50, Sep. 2015.
[13] D. Wang, D. Chen, B. Song, N. Guizani, X. Yu, and X. Du, "From IoT to 5G I-IoT: The next generation IoT-based intelligent algorithms and 5G technologies," *IEEE Commun. Mag.*, vol. 56, no. 10, pp. 114–120, Oct. 2018.
[14] R. Santos, H. Ghazzai, and A. Kassler, "Optimal steerable mmWave mesh backhaul reconfiguration," in *Proc. IEEE Global Commun. Conf. (GLOBECOM)*, Abu Dhabi, UAE, Dec. 2018, pp. 1–7.
[15] S.-W. Jo and W.-S. Shim, "LTE-maritime: high-speed maritime wireless communication based on LTE technology," *IEEE Access*, vol. 7, pp. 53172–53181, 2019.
[16] H. Ghazzai, E. Yaacoub, and M.-S. Alouini, "Optimized LTE cell planning for multiple user density subareas using meta-heuristic algorithms," in *Proc. IEEE 80th Veh. Technol. Conf. (VTC-Fall)*, Sep. 2014, pp. 1–6.
[17] E. J. Oughton, Z. Frias, S. van der Gaast, and R. van der Berg, "Assessing the capacity, coverage and cost of 5G infrastructure strategies: Analysis of The Netherlands," *Telematics Informat.*, vol. 37, pp. 50–69, Apr. 2019. [Online]. Available: http://www.sciencedirect.com/science/article/pii/S073658531830830X
[18] E. Yaacoub and Z. Dawy, "LTE radio network planning with HetNets: BS placement optimization using simulated annealing," in *Proc. MELECON-17th IEEE Medit. Electrotechnical Conf.*, Apr. 2014, pp. 327–333.
[19] H. Ghazzai, E. Yaacoub, M.-S. Alouini, Z. Dawy, and A. Abu-Dayya, "Optimized LTE cell planning with varying spatial and temporal user densities," *IEEE Trans. Veh. Technol.*, vol. 65, no. 3, pp. 1575–1589, Mar. 2016.
[20] (2014). *On LTE Cellular Radio Network Planning Under Demand Uncertainty*. [Online]. Available: http://ieeexplore.ieee.org/stamp/stamp.jsp?tp=&arnumber=6952610
[21] Y. Lv, H. Zhang, and S. Xueming, "Analysis of base stations deployment on power saving for heterogeneous network," in *Proc. IEEE 17th Int. Conf. Commun. Technol. (ICCT)*, Oct. 2017, pp. 1439–1444.
[22] S. K. Goudos, M. Deruyck, D. Plets, L. Martens, K. E. Psannis, P. Sarigiannidis, and W. Joseph, "A novel design approach for 5G massive MIMO and NB-IoT green networks using a hybrid Jaya-differential evolution algorithm," *IEEE Access*, vol. 7, pp. 105687–105700, 2019.
[23] A. L. Rezaabad, H. Beyranvand, J. A. Salehi, and M. Maier, "Ultra-dense 5G small cell deployment for fiber and wireless backhaul-aware infrastructures," *IEEE Trans. Veh. Technol.*, vol. 67, no. 12, pp. 12231–12243, Dec. 2018.
[24] M. Dong, T. Kim, J. Wu, and E. W.-M. Wong, "Millimeter-wave base station deployment using the scenario sampling approach," *IEEE Trans. Veh. Technol.*, vol. 69, no. 11, pp. 14013–14018, Nov. 2020.
[25] R. Chen, X. Zhang, J. Wang, Q. Cui, W. Xu, and M. Pan, "Data-driven small cell planning for traffic offloading with users' differential privacy," in *Proc. ICC-IEEE Int. Conf. Commun. (ICC)*, Dublin, Ireland, Jun. 2020, pp. 1–6.
[26] K. N. R. S. V. Prasad, E. Hossain, and V. K. Bhargava, "Energy efficiency in massive MIMO-based 5G networks: Opportunities and challenges," *IEEE Wireless Commun.*, vol. 24, no. 3, pp. 86–94, Jun. 2017.
[27] G. E. Athanasiadou, G. V. Tsoulos, D. A. Zarbouti, and I. K. Valavanis, "Optimizing radio network planning evolution towards microcellular systems," *Wireless Pers. Commun.*, vol. 106, no. 2, pp. 521–534, May 2019.
[28] M. Masoudi *et al.*, "Green mobile networks for 5G and beyond," *IEEE Access*, vol. 7, pp. 107270–107299, 2019.
[29] R. Bassoli, M. D. Renzo, and F. Granelli, "Analytical energy-efficient planning of 5G cloud radio access network," in *Proc. IEEE Int. Conf. Commun. (ICC)*, May 2017, pp. 1–4.
[30] A. A. Vaganova, N. N. Kisel, and A. I. Panychev, "Simulation model of 5G coverage in urban areas," in *Proc. Radiat. Scattering Electromagn. Waves (RSEMW)*, Jun. 2019, pp. 372–375.
[31] B. Cao, Q. Wei, Z. Lv, J. Zhao, and A. K. Singh, "Many-objective deployment optimization of edge devices for 5G networks," *IEEE Trans. Netw. Sci. Eng.*, vol. 7, no. 4, pp. 2117–2125, Oct. 2020.
[32] E. Oughton, Z. Frias, T. Russell, D. Sicker, and D. D. Cleevely, "Towards 5G: Scenario-based assessment of the future supply and demand for mobile telecommunications infrastructure," *Technol. Forecasting Social Change*, vol. 133, pp. 141–155, Aug. 2018. [Online]. Available: http://www.sciencedirect.com/science/article/pii/S0040162517313525
[33] H. GANAME, L. Yingzhuang, H. Ghazzai, and D. Kamissoko, "5G base station deployment perspectives in millimeter wave frequencies using meta-heuristic algorithms," *Electronics*, vol. 8, no. 11, p. 1318, Nov. 2019, doi: 10.3390/electronics8111318.
[34] S. Dadvandipour and M. Alsharif, "On the analysis and tool development of the long term evolution cell planning," in *Proc. 20th Int. Carpathian Control Conf. (ICCC)*, May 2019, pp. 1–6.
[35] N. Saxena, A. Roy, and H. Kim, "Efficient 5G small cell planning with eMBMS for optimal demand response in smart grids," *IEEE Trans. Ind. Informat.*, vol. 13, no. 3, pp. 1471–1481, Jun. 2017.
[36] M. Jaber, Z. Dawy, N. Akl, and E. Yaacoub, "Tutorial on LTE/LTE—A cellular network dimensioning using iterative statistical analysis," *IEEE Commun. Surveys Tuts.*, vol. 18, no. 2, pp. 1355–1383, 2nd Quart., 2016.
[37] F.-H. Tseng, L.-D. Chou, H.-C. Chao, and J. Wang, "Ultra-dense small cell planning using cognitive radio network toward 5G," *IEEE Wireless Commun.*, vol. 22, no. 6, pp. 76–83, Dec. 2015.
[38] *3GPP TS 38.101-1*, document (TS) 36.331, 10 2018, 3rd Generation Partnership Project (3GPP), Version 15.3.0. [Online]. Available: https://www.3gpp.org/DynaReport/38-series.htm
[39] A. Ghosh, A. Maeder, M. Baker, and D. Chandramouli, "5G evolution: A view on 5G cellular technology beyond 3GPP release 15," *IEEE Access*, vol. 7, pp. 127639–127651, 2019.
[40] S.-Y. Lien, S.-L. Shieh, Y. Huang, B. Su, Y.-L. Hsu, and H.-Y. Wei, "5G new radio: Waveform, frame structure, multiple access, and initial access," *IEEE Commun. Mag.*, vol. 55, no. 6, pp. 64–71, Jun. 2017.
[41] J. Wang, J. Xu, Y. Yang, and H. Xu, "GPP based open cellular network towards 5G," *China Commun.*, vol. 14, no. 6, pp. 189–198, 2017.
[42] P. Banelli, G. Colavolpe, L. Rugini, and A. Ugolini, "Spectral efficiency of multicarrier schemes for 5G," in *Proc. 26th Int. Conf. Telecommun. (ICT)*, Apr. 2019, pp. 124–129.
[43] X. Xu, J. Li, M. Zhou, J. Xu, and J. Cao, "Accelerated two-stage particle swarm optimization for clustering not-well-separated data," *IEEE Trans. Syst., Man, Cybern. Syst.*, vol. 50, no. 11, pp. 4212–4223, Nov. 2020.
[44] C. Wu, M. Wang, B. Ma, and K. Chen, "Heterogeneous networks topology optimization based on simulated annealing algorithm," in *Proc. IEEE 4th Inf. Technol., Netw., Electron. Autom. Control Conf. (ITNEC)*, vol. 1, Jun. 2020, pp. 2074–2078.

**HASSANA GANAME** received the B.S. degree in physics from the University of Mali, in 2005, and the M.S. degree in electronic and information engineering from the Huazhong University of Science and Technology (HUST), Wuhan, China, in 2009, where he is currently pursuing the Ph.D. degree in electronic and information engineering.

**LIU YINGZHUANG** received the Ph.D. degree in communication and information engineering from the Huazhong University of Science and Technology (HUST), China, in 2000. Before, he worked with HUST in 2002, he was a Postdoctoral Researcher with Paris University XI, France. He is currently a Professor with the Department of Electronics and Information Engineering. His research interest includes mobile communication (3G, LTE, and IMT-A).

**AYMEN HAMROUNI** (Student Member, IEEE) received the Diplome d'Ingenieur degree *(summa cum laude)* in telecommunication engineering from the Ecole Superieure des Communications de Tunis (SUP'COM), Tunis, Tunisia, in 2019. In 2019, he worked as a Research Assistant with the Stevens Institute of Technology, Hoboken, NJ, USA. He is currently a Research Scholar with the School of Systems and Enterprises, Stevens Institute of Technology. His research interests include the intersection of mobile crowdsourcing, applied machine learning, optimization, network analysis, mathematical modeling, graph theory, and the Internet-of-Things.

**HAKIM GHAZZAI** (Senior Member, IEEE) received the Diplome d'Ingenieur degree (Hons.) in telecommunication engineering and the master's degree in high-rate transmission systems from the Ecole Superieure des Communications de Tunis (SUP'COM), Tunis, Tunisia, in 2010 and 2011, respectively, and the Ph.D. degree in electrical engineering from KAUST, Saudi Arabia, in 2015. He is currently a Research Scientist with the Stevens Institute of Technology, Hoboken, NJ, USA. Before joining Stevens, he was a Visiting Researcher with Karlstad University, Sweden, and a Research Scientist with the Qatar Mobility Innovations Center, Doha, Qatar, from 2015 to 2018. His research interests include the intersection of wireless networks, UAVs, the Internet-of-Things, intelligent transportation systems, and optimization.

**HUA CHEN** is currently an Associate Professor with Wuhan Textile University. Since 2005, she presided more than three Hubei natural science fund projects, more than two Hubei youth fund projects, and published more than 15 articles in the field of network communications. Her research interests include network communications, including optimization theory and technology.